Acta Crystallographica Section D
Biological Crystallography
ISSN 0907-4449

PRR1 coat protein binding to its RNA translational operator

Magnus Persson,[a] Kaspars Tars[b] and Lars Liljas[a]*

[a]Department of Cell and Molecular Biology, Uppsala University, BMC, Husargatan 3, Box 596, S-751 24 Uppsala, Sweden, and [b]Latvian Biomedical Research and Study Center, Ratsupites 1, Riga, LV 1067, Latvia

Correspondence e-mail: lars@xray.bmc.uu.se

Received 5 September 2012
Accepted 19 November 2012

PDB Reference: PRR1, complex with RNA segment, 4ang

In small RNA bacteriophages, the genomic RNA binds to the coat proteins when the viral capsid assembles. This is achieved through sequence-specific interactions between a coat-protein dimer and an RNA stem-loop that includes the start codon for the replicase gene. The structure of virus-like particles of the small RNA phage PRR1 bound to an RNA segment corresponding to this stem-loop has been solved and the binding was compared with the related, and better investigated, phage MS2. The overall conformation of the RNA is found to be similar and the residues that are involved in RNA binding in PRR1 are the same as in MS2. The arrangement of the nucleotide bases in the loop of the stem-loop is different, leading to a difference in the stacking at the conserved Tyr86, which is equivalent to Tyr85 in MS2.

1. Introduction

Every virus faces the challenge of packaging its own genome in the capsid. One of the most obvious ways of achieving this is by direct sequence-specific interactions between the coat protein and the viral nucleic acid. This approach is used by the small RNA bacteriophages. The coat protein of small RNA bacteriophages forms dimers in which a β-sheet from each subunit is arranged into a continuous large sheet. 90 dimers assemble into $T = 3$ viral capsids (Valegård *et al.*, 1990). The coat-protein dimer specifically binds the genomic RNA at the site of the initiation codon of the viral replicase, thereby regulating the translation of this enzyme. This interaction has been studied extensively in the case of the related small RNA bacteriophage MS2 (Johansson *et al.*, 1997; Witherell *et al.*, 1991). The crystal structure of an MS2 coat-protein complex with an RNA stem-loop has been determined (Valegård *et al.*, 1994).

The quasi-equivalent coat-protein monomers are denoted *A*, *B* and *C* and form two types of dimers: *AB* dimers at the quasi-twofold axes and *CC* dimers at the twofold axes. In MS2 the conformation of the *B* subunit is significantly different from those of the *A* and *C* subunits (Valegård *et al.*, 1990). The difference is mainly found in a loop between β-strands *F* and *G* (the FG-loop), which forms the contacts at the fivefold and quasi-sixfold axes. In the *B* subunit of MS2 the FG-loop is bent inwards, preventing one of the two possible binding modes of the RNA stem-loop to the *AB* dimer. Both binding modes are possible and are observed in the *CC* dimer. The related small RNA bacteriophages fr and GA belonging to the same family, *Leviviridae*, have a similar conformation of the FG-loop in the *B* subunit (Liljas *et al.*, 1994; Tars *et al.*, 1997). In three other phages, PP7 (Tars *et al.*, 2000), PRR1 (Persson *et al.*, 2008) and φCb5 (Plevka *et al.*, 2009), the FG-loop is extended in all three subunits, while in the case of Qβ the FG-loops of the *AB*

dimer are partly disordered (Golmohammadi *et al.*, 1996). In Qβ and PP7 the FG-loops are connected *via* cystine bridges that make the loops more rigid. This rigidity makes it much more difficult for the RNA stem-loops to enter the shell of recombinantly expressed virus-like particles (VLPs) during soaking or cocrystallization experiments. A better candidate for this is PRR1, which lacks disulfides. An alternative to soaking recombinant VLPs with RNA is to form complexes with coat-protein mutants that are unable to form capsids. This approach has been successful for PP7 (Chao *et al.*, 2008).

A comparison of several *Leviviridae* coat proteins shows that many of the residues that are involved in RNA binding in MS2 are conserved both in amino-acid sequence and three-dimensional structure (Persson *et al.*, 2008). The binding surface is similar, although they bind stem-loops with different conformations and loop sizes ranging from three to six nucleotides (Gott *et al.*, 1991; Witherell *et al.*, 1991; Witherell & Uhlenbeck, 1989). In MS2, two adenine bases, one from the loop and one bulged base from the stem, bind in the corresponding pockets in the two protein subunits of the dimer and another base in the loop stacks on a tyrosine in one of the subunits. There are also a number of interactions with the RNA backbone (Valegård *et al.*, 1994). However, the complex between the PP7 coat-protein dimer and RNA showed a different binding mode that utilizes different adenine-binding pockets to those used in MS2 (Chao *et al.*, 2008). This indicates that the *Leviviridae* phages may use the same coat-protein scaffold to specifically bind different RNA operators with different binding modes.

In this study, the structure of recombinantly expressed wild-type PRR1 VLPs in complex with a wild-type RNA stem-loop bound to the coat-protein *AB* and *CC* dimers has been solved to a resolution of 3.5 Å. The binding mode of the PRR1 coat protein to the RNA stem-loop is similar to that of MS2, but the RNA is bound in two orientations to both the *AB* and the *CC* dimers.

2. Materials and methods

The PRR1 VLPs were expressed and purified as described by Persson *et al.* (2008). The RNA oligonucleotide (5′-CCA-UAAGGAGCUACCUAUGG-3′) used for cocrystallization experiments was ordered from DNA Technology A/S, Denmark. Crystals were obtained by the hanging-drop vapour-diffusion technique. The reservoir solution consisted of 25 µ*M* $CaCl_2$, 100 m*M* bis-tris pH 6.5, 20% PEG 550 monomethylether. The drop consisted of a 1:1:1 volume ratio of PRR1 coat-protein solution at 10 mg ml^{-1} in 20 m*M* Tris–HCl pH 8.0, reservoir solution and 3 m*M* aqueous RNA solution. Reservoir solution containing 30% PEG 550 monomethylether was used as cryoprotectant. Data were collected on beamline ID14-1 at the European Synchrotron Radiation Facility, Grenoble, France.

Data from a single crystal were processed and scaled using the *HKL*-2000 package (Otwinowski, 1993). The space group was identified as *P*1 and the unit-cell parameters were $a = 281.3$, $b = 285.4$, $c = 472.9$ Å, $\alpha = 93.23$, $\beta = 90.03$, $\gamma = 119.45^\circ$. The unit cell and the asymmetric unit contained two particles. The unit cell is very similar to that obtained for the PRR1 VLP (Persson *et al.*, 2008). The PRR1 VLP model (PDB entry 2vf9) was used as a phasing model. The program *GLRF* (Tong & Rossmann, 1990) was used to find the orientation of the particles. A locked rotation function was calculated using data between 10 and 7 Å resolution. Phases from the model were calculated in *CNS* (Brünger *et al.*, 1998) and were combined with the observed amplitudes. Real-space averaging was performed using the 120-fold NCS of the icosahedral particles in *AVE* (Kleywegt & Jones, 1994) until the correlation coefficient converged. The particle positions and orientations were optimized using cyclic real-space averaging. Each parameter was changed stepwise and the total correlation coefficient using all reflections was used to select the best value for each parameter. The procedure was repeated until no improvement occurred. The particle positions were 0.0 0.0 0.0 (fixed) and 0.498 −0.060 0.475. The differences in unit-cell parameters, particle positions and orientations between the crystals with and without bound RNA were all very small and the use of the optimized parameters did not significantly improve the electron-density map.

The electron-density map after this optimization was used for model building in the program *O* (Jones *et al.*, 1991), and *CNS* was used for the final refinement of the coordinates and temperature factors. Alternative conformations of the bound RNA were included in the refinement with suitable occupancies and relevant restrictions were applied to avoid technical problems with atoms occupying similar positions in the alternative conformations. The coordinates and structure-factor amplitudes have been deposited in the PDB (entry 4ang).

3. Results

3.1. PRR1 RNA binding

There is clear electron density for the backbone and side chains of the *A*, *B* and *C* coat-protein subunits. The overall shape of the RNA could also easily be followed, with the exception of parts of the loop region (see below) and the three base pairs at the 3′ and the 5′ ends of the RNA molecule. A single RNA molecule binds to a coat-protein dimer. The dimer has perfect (*CC* dimer) or approximate (*AB* dimer) twofold symmetry, and both orientations of the RNA molecule at the twofold (*CC* dimer) and quasi-twofold (*AB* dimer) axes are observed in the electron-density map; the molecules partly occupy the same space. It was obvious from the map that the RNA binds to the coat protein in a similar way as in MS2 and most of the nucleotides in the RNA stem-loops could be modelled in the density. In the *AB* dimer both conformations of the RNA were modelled. In the *CC* dimer only one of the RNA binding conformations was modelled owing to the exact twofold symmetry. The occupancy of the RNA molecules were chosen such that the temperature factors of the adenine bases A−4 and A−11 were similar to the temperature factors of the protein side chains that form their binding pockets. The

resulting occupancies varied between 0.35 and 0.45. The final model had an *R* value of 0.31 (Table 1). Electron-density maps of particles without added RNA (Persson *et al.*, 2008) did not show any significant density for nonspecifically bound RNA molecules.

The general shape of the bound RNA is similar to the MS2 RNA (Valegård *et al.*, 1997), but in contrast to the MS2 RNA the PRR1 stem-loop binds to the *AB* dimer in two orientations. The basis of this difference is that the extended FG-loops of the *A*, *B* and *C* subunits do not interfere with the binding of the stem-loop. Fig. 1 shows the PRR1 and MS2 stem-loops and Fig. 2(*a*) shows the model of the stem-loop bound to an *AB* dimer of PRR1. Both orientations are illustrated. Fig. 2(*b*) shows the corresponding model of the MS2 stem-loop, in which the conformation of the FG-loop of the *B* subunit prevents the stem-loop from binding in the other orientation. In PRR1, nucleotides U−13 to G−7 exhibit a base-stacking arrangement, with the exception of the bulged A−11, where the base points towards the protein. The bases stack on Tyr*A*86. A tyrosine is also found in the corresponding position in MS2 and has been shown to be important for the pH dependence of K_d (LeCuyer *et al.*, 1996). The loop consists of A−8 to A−4, where C−6, U−5 and A−4 are not involved in base stacking (Fig. 2*c*). The density is weak and not interpretable for nucleotide U−5 and the base of nucleotide C−6.

The conformation of the loop of the RNA molecule bound to the *CC* dimer is different, with the base of nucleotide U−5 replacing the base of G−7 stacking with Tyr*C*86 (Fig. 2*c*). In this RNA molecule, nucleotide C−6 and the base of G−7 are impossible to interpret because of weak and unconnected density.

The coat protein recognizes the correct RNA through a number of specific interactions (Fig. 3). The coat protein has a pocket in which exposed bases can bind. This pocket has a preference for adenine bases. In the dimer, there are two symmetry-related pockets in which the adenine bases of A−4 and A−11 make specific interactions with the coat protein. Both form hydrogen bonds to Thr46 and Ser48. From the 5′ end to A−11 the RNA bends away from the protein and no interactions are observed.

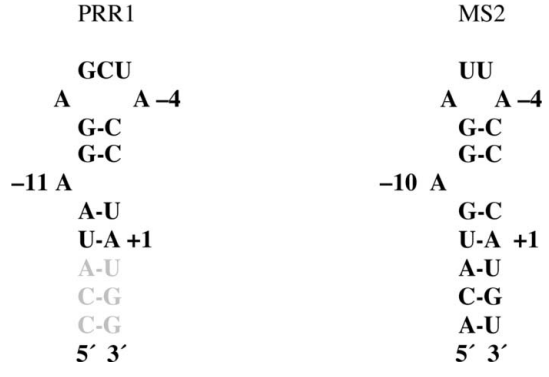

Figure 1
RNA stem-loop structures of PRR1 and MS2. The number +1 signifies the start codon of the replicase gene. The three base pairs at the lower end of the stem (shown in grey) were not included in the final model owing to a lack of density.

Table 1
Data-collection and refinement statistics.

Resolution (Å)	50.0–3.5
No. of measured reflections	323076
No. of unique reflections	259990
Completeness (%)	16
R_{merge} (overall)	0.131
R_{merge} (50–7.53 Å)	0.054
R_{merge} (3.63–3.50 Å)	0.390
Space group	*P*1
Unit-cell parameters (Å, °)	a = 281.3, b = 285.4, c = 472.9, α = 93.23, β = 90.03, γ = 119.45
R factor (30–3.50 Å)	0.31

The coat protein with bound RNA shows little difference in comparison to the empty particle. There are two residues, Arg50 and Asn54, where a significant difference is found that can be related to RNA binding. One of the side-chain N atoms of Arg50 would be too close to a phosphate O atom of G−9. The Arg50 side chain therefore has to adopt a somewhat different conformation in the complex. The electron density for the side chain of Arg50 is also noticeably stronger in the model with RNA compared with the model without RNA. The movement of the Asn54 side chain is likely to be necessary to accommodate the RNA in the larger loop region of PRR1.

3.2. Structural comparison of RNA binding in PRR1 and MS2

The conformation of the bound RNA and its interaction with the coat-protein dimer are similar in PRR1 and MS2. The amino-acid sequences of MS2 and PRR1 are 26% identical, and many of the conserved residues are found on the RNA-binding surface. A detailed comparison of the RNA–coat protein interactions in PRR1 and MS2 can be found in Table 2 and Fig. 3. The interactions at the adenine-binding pockets are very similar. The conserved residues Ser48 and Thr46 form similar hydrogen bonds to the bases, and Val29 and Lys62 stack on the base and form two walls of the pocket. The lysine has two possible conformations in MS2 (Grahn *et al.*, 1999; Rowsell *et al.*, 1998). Owing to weak density, the exact position of this lysine in PRR1 is not clear, but there is also support in the density for two conformations in PRR1. One of the conformations was chosen for the model.

Both viruses also make use of the tyrosine-stacking interaction, where only one of the symmetry-related side chains is used in each complex. In MS2 an additional hydrogen bond from the tyrosine hydroxyl is found. The A−8, G−9 and A−11 nucleotides in PRR1 and the equivalent nucleotides A−7, G−8 and A−10 in MS2 interact similarly with the protein. In MS2, the RNA hairpin loop is shorter and consists of A−7 to A−4. The base of U−6 points away from the protein, while the base of U−5 forms stacking interactions with Tyr*A*85 and the base of A−7. In PRR1 there is one extra base in this region, which causes the hairpin to extend further towards the protein. The change of Asn87 in MS2 to threonine in PRR1 leaves more space for the larger loop in PRR1. Glu*A*63 in MS2, which interacts with the hydroxyl group of U−5, is replaced by a valine in PRR1. This change causes the polar interaction with the RNA at this position to be lost.

In MS2, a loop in the *B* subunit interacts with the RNA through Ser*B*51, Ser*B*52 and Asn*B*55. In PRR1, the conformation of the corresponding loop is different. Thr52, which corresponds to Ser51 in MS2, interacts with the RNA backbone. There is no significant density for the side chain of Asn54, which is in a position where it could interact with the RNA.

4. Discussion

RNA binding in the small RNA bacteriophage MS2 has been studied thoroughly using biochemical methods as well as X-ray crystallography (LeCuyer *et al.*, 1995; Peabody, 1993; Valegård *et al.*, 1994; Witherell *et al.*, 1991). In contrast, little is known about the RNA binding of other small RNA bacteriophages. The single exception is the structure of a PP7 coat-protein dimer binding to its RNA operator hairpin (Chao *et al.*, 2008). The PP7 structure revealed a different binding mode with different adenine-binding pockets compared with MS2 or PRR1. The binding of Qβ RNA has also been studied in mutants of the MS2 coat protein with a changed specificity (Horn *et al.*, 2006). The Qβ RNA stem-loop has a loop of only three nucleotides and three base pairs between the loop and the bulged adenine, but it is bound very similarly to the MS2 stem-loop. This is possible through a slight change in the orientation of the bases forming pairs in the stem.

In MS2, the importance of the nucleotide type at position −5 has been investigated (Grahn *et al.*, 2000, 2001; Lim *et al.*, 1994; Valegård *et al.*, 1997). The results indicated that the stacking interaction with Tyr*A*85 is the major contributor to

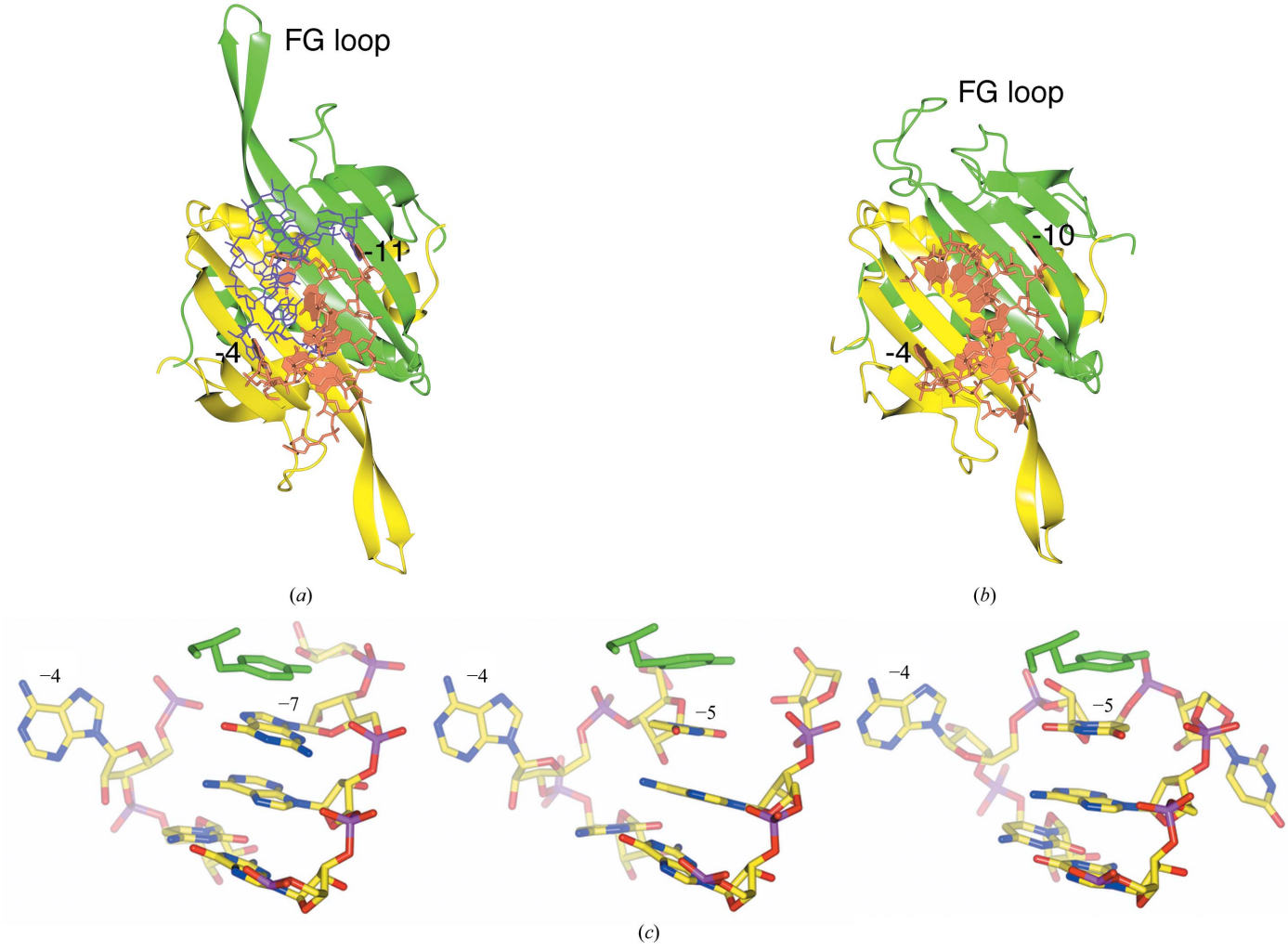

Figure 2
(*a*) The PRR1 RNA stem-loop bound to the *AB* dimer. The stem-loop is shown in both of its two possible orientations. The stem-loops are shown in different representations and colours. The coat-protein dimer is shown with the *A* subunit in yellow and the *B* subunit in green. The exposed bases A−11 and A−4 bound in similar pockets in the *A* and *B* subunits are labelled. The disordered part of the loop connects the two free ends at the lower left part of the RNA. (*b*) The MS2 stem-loop bound to the *AB* dimer. (*c*) The loop region of the stem-loop bound to the *AB* dimer (left), to the *CC* dimer (middle) and to the *AB* dimer of MS2 (right). The two conformers bound to the *AB* dimer in PRR1 are very similar and only one is shown. The loop conformation is different between the stem-loops bound to the *AB* and *CC* dimers in PRR1. Different bases, −7 and −5 in the *AB* and *CC* dimers, respectively, stack with Tyr86. Two bases and part of the RNA backbone could not be modelled in any of the RNA molecules in PRR1 owing to a lack of interpretable density. Owing to the difference in conformation, bases −5 and −6 in the *AB* dimer and bases −6 and −7 in the *CC* dimer were not modelled. The complete loop could be modelled in MS2.

Table 2
Interactions between the RNA stem-loop and the coat protein in PRR1 and MS2 (PDB entry 1zdi).

NP, nonpolar contact. C^2, the *C* subunit related by the twofold axis.

PRR1					MS2		
Nucleotide	Residues	Contacts (*AB*1)†	Contacts (*AB*2)	Contacts (*CC*)	Nucleotide	Residues	Contacts
					G−11	Lys*B*61	NZ–OP2
A−11	Val29	Val*B*29 NP–base	Val*A*29 NP–base	Val$C^2$29 NP–base	A−10	Val*B*29	NP–base
	Thr46	Thr*B*46 OG1–N1	Thr*A*46 OG1–N1	Thr$C^2$46 OG1–N1		Thr*B*45	OG1–N6
	Ser48	Ser*B*48 OG–N3	Ser*A*48 OG–N3	Ser$C^2$48 OG–N3		Ser*B*47	OG1–N1, OG–N3
	Lys62	Lys*B*62 NZ–OP2 (alt), NP–base (alt)	Lys*A*62 NZ–OP1, NP–base	Lys$C^2$62 NZ–OP2, NP–base		Lys*B*61	NZ–OP2
G−9	Arg50	Arg*B*50 NE–OP2	Arg*A*50 NE–OP2	Arg$C^2$50 NE–OP2	G−8	Arg*B*49	NE–OP2, NH2–OP1
A−8	Lys58	Lys*B*58 NZ–OP2	Lys*A*58 NZ–OP2	Lys$C^2$58 NZ–OP2	A−7	Lys*B*57	NZ–OP1
		Asn*B*54 ND2–O3′		Asn$C^2$54 ND2–O5′		Asn*B*55	ND2–OP2
		Thr*B*52 OG1–OP1	Thr*A*52 OG1–OP1	Thr$C^2$52 OG1–OP1		Ser*B*52	OG1–OP2
G−7	Tyr86	Tyr*A*86–base stacking	Tyr*B*86–base stacking	Not visible (except P)			
C−6		Not visible	Not visible	Not visible	U−6	Asn*B*55	ND2–P1
U−5		Not visible	Not visible	Tyr*C*86–base stacking	U−5	Glu*A*63	OE2–O2
						Asn*A*87	ND2–O2
						Tyr*A*85	OH–OP1 stacking
A−4	Val29	Val*A*29 NP–base	Val*B*29 NP–base	Val*C*29 NP–base	A−4	Val*A*29	NP–base
	Thr46	Thr*A*46 OG1–N7	Thr*B*46 OG1–N7	Thr*C*46 OG1–N7		Thr*A*45	OG1–N7
		Thr*A*46 OG1–N6	Thr*B*46 OG1–N6	Thr*C*46 OG1–N6		Thr*A*45	OG1–N6
	Ser48	Ser*A*48 OG–N1	Ser*B*48 OG–N1	Ser*C*48 OG–N1		Ser*A*47	OG–N1
	Thr60	Thr*A*60 O–N6	Thr*B*60 O–N6	Thr*C*60 O–N6		Thr*A*59	O–N6
	Lys62		NP–base	NP–base			
	Arg44	Arg*A*44 NH1–OP1	—	—		Lys*A*43	NZ–OP1

† In PRR1, there are two slightly different conformations of the *AB* dimer and a single conformation of the *CC* dimer. In MS2, only the contacts found in the single mode of binding to the *AB* dimer are shown. The binding to the *CC* dimer is similar.

the coat protein–RNA interaction at this position. In the study by Grahn *et al.* (2001), it was found that the additional hydrogen bonds made by the −5 nucleotide to the protein were of less significance. In PRR1, the loop conformation differs between the bound RNA molecules. The molecule bound to the *CC* dimer has a conformation that is more similar to that of MS2, with U−5 stacked with the tyrosine, while G−7 is stacked in the RNA bound to the *AB* dimer. Both these bases make no additional bonds, indicating the importance of the stacking interaction for binding. The hydrogen bond between Asn*A*87 and U−5 in MS2 is likely to be missing in PRR1 since the Thr at the equivalent position is too far from the base.

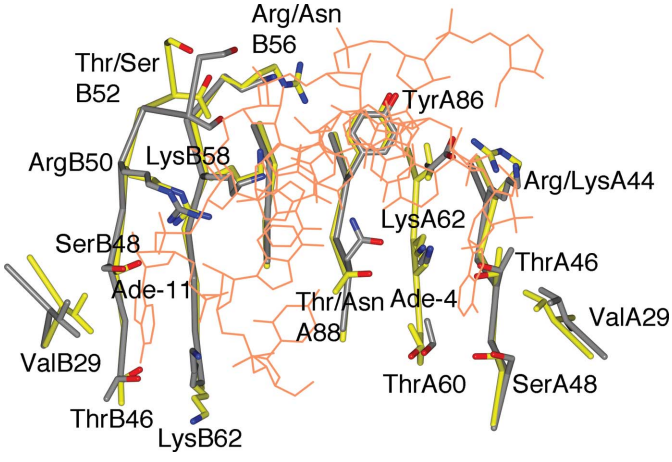

Figure 3
Comparison of the RNA-binding surfaces of the *AB* dimer of MS2 (PDB entry 1zdi) and PRR1. The C^{α} trace and C atoms of PRR1 are shown in yellow and those of MS2 are shown in grey. The RNA molecule of PRR1 (in one orientation) is shown in orange. When the residues differ, the PRR1 residue is mentioned first. The numbering is according to PRR1.

Differences in the loop-binding area that may allow the binding of a larger loop are the replacement of Gln*A*40 in MS2 by Gly41 in PRR1 and of Tyr*A*42 in MS2 by Ala43 in PRR1. A possible explanation of why part of the loop in PRR1 is not observed in the electron density is that it can bind in more than one conformation. The density for the RNA is generally weak since some dimers bind no RNA and the rest bind the RNA stem-loop in two different orientations. The reason for the differences in conformation between RNA molecules bound to the *AB* and *CC* dimers is not obvious. In the particle, the dimers are tightly packed in a way that leads to slightly different orientations. The binding surface available for the RNA molecule is limited not only by the dimer to which it binds but also by a loop in the neighbouring dimer. However, there is no direct interaction with this loop that explains the differences in conformation.

When bound to the coat protein, the stem-loop of PRR1 exhibits a conformation that is similar to that of MS2. The major differences are found in the area of the loop. Differences between the binding sites in the PRR1 particle lead to different conformations of the loop in the PRR1 stem-loop itself. The stacking interaction with Tyr*A*86 is retained. In one of the observed conformations the stacking base corresponds to the base in MS2, but in the other conformations another base from the loop stacks with the tyrosine side chain.

This work was supported by the Swedish Research Council and ERDF grant 2DP/2.1.1.1.0/10/APIA/VIAA/052. We

would also like to thank the staff at ESRF for their support and Pavel Plevka for collecting the data.

References

Brünger, A. T., Adams, P. D., Clore, G. M., DeLano, W. L., Gros, P., Grosse-Kunstleve, R. W., Jiang, J.-S., Kuszewski, J., Nilges, M., Pannu, N. S., Read, R. J., Rice, L. M., Simonson, T. & Warren, G. L. (1998). *Acta Cryst.* D**54**, 905–921.

Chao, J. A., Patskovsky, Y., Almo, S. C. & Singer, R. H. (2008). *Nature Struct. Mol. Biol.* **15**, 103–105.

Golmohammadi, R., Fridborg, K., Bundule, M., Valegård, K. & Liljas, L. (1996). *Structure*, **4**, 543–554.

Gott, J. M., Wilhelm, L. J. & Uhlenbeck, O. C. (1991). *Nucleic Acids Res.* **19**, 6499–6503.

Grahn, E., Moss, T., Helgstrand, C., Fridborg, K., Sundaram, M., Tars, K., Lago, H., Stonehouse, N. J., Davis, D. R., Stockley, P. G. & Liljas, L. (2001). *RNA*, **7**, 1616–1627.

Grahn, E., Stonehouse, N. J., Adams, C. J., Fridborg, K., Beigelman, L., Matulic Adamic, J., Warriner, S. L., Stockley, P. G. & Liljas, L. (2000). *Nucleic Acids Res.* **28**, 4611–4616.

Grahn, E., Stonehouse, N. J., Murray, J. B., van den Worm, S., Valegård, K., Fridborg, K., Stockley, P. G. & Liljas, L. (1999). *RNA*, **5**, 131–138.

Horn, W. T., Tars, K., Grahn, E., Helgstrand, C., Baron, A. J., Lago, H., Adams, C. J., Peabody, D. S., Phillips, S. E., Stonehouse, N. J., Liljas, L. & Stockley, P. G. (2006). *Structure*, **14**, 487–495.

Johansson, H. E., Liljas, L. & Uhlenbeck, O. C. (1997). *Semin. Virol.* **8**, 176–185.

Jones, T. A., Zou, J.-Y., Cowan, S. W. & Kjeldgaard, M. (1991). *Acta Cryst.* A**47**, 110–119.

Kleywegt, G. J. & Jones, T. A. (1994). *Proceedings of the CCP4 Study Weekend. From First Map to Final Model*, edited by S. Bailey, R. Hubbard & D. Waller, pp. 59–66. Warrington: Daresbury Laboratory.

LeCuyer, K. A., Behlen, L. S. & Uhlenbeck, O. C. (1995). *Biochemistry*, **34**, 10600–10606.

LeCuyer, K. A., Behlen, L. S. & Uhlenbeck, O. C. (1996). *EMBO J.* **15**, 6847–6853.

Liljas, L., Fridborg, K., Valegård, K., Bundule, M. & Pumpens, P. (1994). *J. Mol. Biol.* **244**, 279–290.

Lim, F., Spingola, M. & Peabody, D. S. (1994). *J. Biol. Chem.* **269**, 9006–9010.

Otwinowski, Z. (1993). *Proceedings of the CCP4 Study Weekend. Data Collection and Reduction*, edited by L. Sawyer, N. Isaacs & S. Bailey, pp. 56–62. Warrington: Daresbury Laboratory.

Peabody, D. S. (1993). *EMBO J.* **12**, 595–600.

Persson, M., Tars, K. & Liljas, L. (2008). *J. Mol. Biol.* **383**, 914–922.

Plevka, P., Kazaks, A., Voronkova, T., Kotelovica, S., Dishlers, A., Liljas, L. & Tars, K. (2009). *J. Mol. Biol.* **391**, 635–647.

Rowsell, S., Stonehouse, N. J., Convery, M. A., Adams, C. J., Ellington, A. D., Hirao, I., Peabody, D. S., Stockley, P. G. & Phillips, S. E. (1998). *Nature Struct. Biol.* **5**, 970–975.

Tars, K., Bundule, M., Fridborg, K. & Liljas, L. (1997). *J. Mol. Biol.* **271**, 759–773.

Tars, K., Fridborg, K., Bundule, M. & Liljas, L. (2000). *Virology*, **272**, 331–337.

Tong, L. & Rossmann, M. G. (1990). *Acta Cryst.* A**46**, 783–792.

Valegård, K., Liljas, L., Fridborg, K. & Unge, T. (1990). *Nature (London)*, **345**, 36–41.

Valegård, K., Murray, J. B., Stockley, P. G., Stonehouse, N. J. & Liljas, L. (1994). *Nature (London)*, **371**, 623–626.

Valegård, K., Murray, J. B., Stonehouse, N. J., van den Worm, S., Stockley, P. G. & Liljas, L. (1997). *J. Mol. Biol.* **270**, 724–738.

Witherell, G. W., Gott, J. M. & Uhlenbeck, O. C. (1991). *Prog. Nucl. Acid Res. Mol. Biol.* **40**, 185–220.

Witherell, G. W. & Uhlenbeck, O. C. (1989). *Biochemistry*, **28**, 71–76.